Growth of first generation dendrons on SiO_2: controlling chemisorption of transition metal coordination complexes

Manish Sharma, Abhishek Dube, and James R. Engstrom*

School of Chemical and Biomolecular Engineering

Cornell University

Ithaca, New York 14853

Supporting Information (27 pages)

*Address correspondence to this author: jre7@cornell.edu

Supporting Information

(section numerals correspond to section in main document)

S.II Experimental Procedures

S.II.A Formation of generation 0 and generation 1 interfacial organic layers (IOLs)

Materials – 3-aminopropyldimethylethoxysilane and 11-cyanoundecyltrichlorosilane, generation 0 precursors, were purchased from Gelest, Inc. (Morrisville, PA) and used as received. The following chemicals, used for depositing generation 0 and growing generation 1 layers, were purchased from Sigma-Aldrich Corp. (St. Louis, MO): toluene**,** anhydrous, 99.8%; bicyclohexyl, 99%; 1.0 M borane-tetrahydrofuran (BH_3-THF) complex; 37% hydrochloric acid, A.C.S. reagent; terahydrofuran (THF), >99%, A.C.S. reagent; methyl acrylate, >99%, stabilized; and ethylene diamine, >99.5%, redistilled. All these chemicals were used as received except bicyclohexyl and THF which were dried immediately before use using 8 mesh Drierite (W.A. Hammond Drierite Co. Ltd., Xenia, OH). Methanol, 99.9%, anhydrous, was purchased from Alfa-Aesar (Ward Hill, MA). Chloroform, 99.8%, HPLC grade with 50 ppm pentene, obtained from Fisher Scientific International Inc. was used to sonicate freshly cleaved Si wafers. The following chemicals were used as received from Mallinckrodt Baker Inc. (Phillipsburg, NJ): CMOS^{TM} grade acetone, CMOS^{TM} grade 2-propanol, and buffered oxide etch (BOE, 6:1 CMOS^{TM} grade NH_4F-HF aqueous solution). Nanostrip, a stabilized solution of H_2SO_4 and H_2O_2, was received from Cyantek Corp. (Freemont, CA) and used as received.

Substrate Preparation – Si (100) wafers, 100mm, single side polished, 500-550 μm thick, doped with B to a resistivity of 38-63 Ω-cm, were used as starting substrates. They were cleaved to a size of 16.75 × 16.75 mm^2, sonicated in chloroform and dried with N_2. Immediately thereafter, the wafers were dipped in BOE for 1 min., rinsed with de-ionized (DI) water and dried with N_2. A thin layer of silicon dioxide (so called "chemical oxide") was grown by placing the samples in Nanostrip solution for 15 min. at 75 °C. After rinsing the samples with DI water and drying them with N_2, BOE/Nanostrip treatment was repeated for a second time. This procedure consistently produces a chemical oxide on Si substrates with a thickness of 15-20 Å and the surface is fully wet by water with an advancing as well as receding contact angles of 0° [1]. This oxide has been reported to possess SiOH groups in a density ~ 5 × 10^{14}-cm^{-2} [2, 3] and is the "chemical oxide" referred to below.

Formation of generation 0 IOLs – Two types of generation 0 IOLs were formed on chemical oxide in this work with the purpose of using them as two different anchors to grow branched overlayers or generation 1 IOLs. The shorter/thinner generation 0 IOL was formed using 3-aminopropyldimethylethoxysilane precursor, $(C_2H_5O)(CH_3)_2Si(CH_2)_3NH_2$, which is referred to as 3C below. A 1% solution (v/v) of 3C was made in toluene and the samples with freshly deposited chemical oxide were kept in this solution for 12 hours. After the silanization, the samples were washed with toluene and baked for 30 min. at 120 °C. Subsequently the substrates were sonicated in toluene, a mixture of toluene and methanol (v/v=1/1) and methanol. Each sonication step was carried out for 2 min. The samples were then dried in N_2 and used for further processing. This method has been reported to consistently produce a monolayer of 3C with 6-12 hours of deposition time.[4] The ellipsometric thickness of the IOL obtained using 3C as

the precursor, has been reported to be very close to the calculated value of molecular length for 3C [4] (a monoethoxysilane). This is unlike the IOLs formed using its diethoxy or triethoxy analogues, possibly due to their forming a cross-linked structure on the surface.

The longer/thicker IOL was formed using 11-cyanoundecyltrichlorosilane as the precursor, $(Cl)_3Si(CH_2)_{11}CN$, referred to as 12C here. A 2.5 mM solution of 12C was prepared with bicyclohexyl as the solvent and the substrates having a chemical oxide film were dipped in this solution for 3 min. at ~ 6 °C. The solvent was chosen by taking into account its freezing point and the transition temperature to be maintained for the formation of well-ordered IOLs [5]. Post deposition, the samples were sonicated in anhydrous chloroform for 15 min. to remove any polymerized residue. Finally, they were rinsed with DI water and dried with N_2. Following this, the –CN termination of the IOL ($\equiv Si\text{-}(CH_2)_{11}\text{-}CN$) was converted into an $–NH_2$ termination ($\equiv Si\text{-}(CH_2)_{11}\text{-}CH_2NH_2$) by a four hour dip in 1.0M BH_3-THF solution, followed by a 1 hour dip in methanol and a 15 min. dip in 10% HCl. This treatment has been reported to reduce the –CN group completely. [6] The samples were cleaned with DI water and dried with N_2 before further processing.

Growth of generation 1 IOLs – Two sequential reaction steps were performed in order to grow branched overlayers on generation 0 IOLs (which were formed as mentioned above) to obtain generation 1 IOLs. In the first step, the substrates with the $–NH_2$ terminated generation 0 IOLs were immersed in a 1/1 (v/v) methyl acrylate/methanol solution for ~ 24 hours at room temperature. After withdrawal, they were washed with methanol and transferred to a 1/1 (v/v) ethylenediamine/methanol solution at 50 °C. This second step was carried out for ~ 18 hours after which the samples were taken out and washed with methanol, dried with N_2 and used for

analysis and further processing. This reaction strategy is similar to the divergent type solvent phase synthesis of polyamidoamine (PAMAM) dendrimers. [7] The first step – Michael addition of an ester – introduces branching at the terminal 'N' position of the starting substrate by adding two acrylate molecules to each $–NH_2$ group while the second step – amidation of the resulting ester moieties with an excess of alkylene diamine – gives back $–NH_2$ termination [7-9].

S.II.B. Characterization of the self assembled monolayers

Contact angle measurements – A NRL CA Goniometer (Rame-Hart Inc., Mountain Lakes, NJ) was used to perform contact angle measurements on generation 0 and generation 1 IOLs for both starting anchors. Contact angles were measured using an advancing droplet volume of at least 3 μL and the receding droplet volume of ~ 2 μL. The measurements were performed on each side of the droplet on at least three different locations on the surface and the average of these values is reported.

Ellipsometry – The thickness of the IOLs was measured using a Rudolph AutoEL-II ellipsometer equipped with a He-Ne (632.8 nm) laser light source incident at 70° with respect to the surface normal. A value of 1.46 has been reported for the refractive index of chemical oxide[10] while for the IOL precursors used here, the refractive index for the bulk phase has been reported as 1.42-1.44 [3, 4]. A refractive index of 1.46 was used in this work for composite layers – chemical oxide/generation 0 and chemical oxide/generation 0/generation 1 IOLs. The sensitivity of the measured thickness to the value assumed for refractive index was small – a change of 0.05 in the latter resulted in less than 1 Å change in the former. The measurements were taken at 4

different spots on each sample with 5 samples used for each stage of the synthesis. Specifically, the thickness values for generation 0 IOLs of 3C and 12C reported here are the average increase in thicknesses in going from chemical oxide to generation 0 in each case. Similarly, the thickness of the generation 1 IOLs is the average increase in thickness in going from chemical oxide to generation 1 IOLs. The estimated error in these measurements is ± 2 Å.

X-ray photoelectron spectroscopy (XPS) – A VSW twin anode x-ray source (Mg/Al) and a VSW CLASS 100 concentric hemispherical energy analyzer (VSW Worldwide, Cheshire, U.K.) were used to carry out XP spectroscopy. All the spectra in this work were obtained using Mg Kα x-rays (1253.6 eV). Survey scans (0-1226 eV) were carried out in the fixed retardation ratio mode whereas detailed scans (range of ~ 20 eV for a specific feature) were carried out in the fixed analyzer transmission mode. The emission current for the source was kept constant at 20 mA and the electrode voltage at 12 kV. The take-off angle for photoelectrons was 38.5 with respect to the surface normal for all XPS scans (analysis area 5 mm diameter) with the take-off angle varied between 0° and 60 for acquiring angle resolved XPS scans (analysis area 1 × 10 mm^2 rectangle). A background subtraction method first proposed by Shirley [11] was used in the analysis of all peaks. Peak areas and peak positions were obtained by fitting the spectra to a product Gaussian-Lorentzian (G-L) function with a mixing ratio of 0.9. [12, 13]

Atomic Force Microscopy (AFM) - Images were acquired with a Dimension 3100 scanning probe microscope (Veeco Instruments, Woodbury, NY) in tapping mode using Tap 300 SPM probes (Nanodevices Inc., Santa Barbara, CA). Typical images obtained were of size 0.5 × 0.5 μm^2 and subjected to a second order plane fit using Nanoscope software (v 5.0).

S.II.C. Study of the reaction of $Ta[N(CH_3)_2]_5$ with generation 0 and generation 1 IOLs

UHV Apparatus – Gas surface reactions between $Ta[N(CH_3)_2]_5$ or $Ti[N(CH_3)_4]$ and generations 0 and 1 IOLs were carried out in a custom designed UHV chamber described elsewhere in detail[14]. The following refers to experiments involving $Ta[N(CH_3)_2]_5$, conditions specific to the use of $Ti[N(CH_3)_4]$ can be found elsewhere. [15] A microcapillary array doser (Burle Technologies Inc.. Lancaster, PA) made of lead silicate glass (0.3 mm thick, 18 mm diameter of capillary, 5 μm pore size, 6 μm center to center spacing with solid border) was used to deliver a constant flux of $Ta[N(CH_3)_2]_5$ to the surface of the sample, without producing a significant rise in the background pressure of the UHV chamber. The doser was kept 25.4 mm from the center of the sample during exposures. A ¼ in. silver plated SS gasket with an aperture 178.8 μm in diameter and 125 ± 25 μm in length was placed between the $Ta[N(CH_3)_2]_5$ bubbler (a sealed stainless steel vessel containing $Ta[N(CH_3)_2]_5$) and the doser and used as a flow limiting orifice. The $Ta[N(CH_3)_2]_5$ bubbler was kept at 9-12 °C. At this temperature the partial pressure of $Ta[N(CH_3)_2]_5$ measured using a capacitance manometer on the line connecting the bubbler to the doser was found to be < 0.001 Torr. In order to estimate the throughput of $Ta[N(CH_3)_2]_5$ to the chamber, we calculated the conductance of the tubing connecting the capacitance manometer, the flow limiting aperture and the capillary array. This, when coupled with the pressure of the chamber and the measured partial pressure of $Ta[N(CH_3)_2]_5$ gave a flux for $Ta[N(CH_3)_2]_5$ of 1.184×10^{12} molecules-cm^{-2}-s^{-1}.

Experimental Procedure – A substrate possessing a specific IOL (generation 0 or 1 of 3C or 12C) was introduced into the ultrahigh vacuum chamber via the fast entry load- lock. Once the pressure was ~ 3.5×10^{-8} Torr, XPS scans were initiated. The survey scan was performed followed by N(1s), C(1s), O(1s) and Si(2p) scans to verify IOL identity and quantify coverage. A spectrum in the range of Ta(4f) feature was also obtained to compare with the post $Ta[N(CH_3)_2]_5$ exposure scan of the same. A small peak corresponding to the O(2s) feature was observed in this binding energy range for pre-exposure scans. To strip this contribution from subsequent scans of the Ta(4f) peak after exposure to $Ta[N(CH_3)_2]_5$ the following procedure was used. For the post exposure scans in the Ta(4f) binding energy region, the O(2s) peak at ~26 eV binding energy was assumed to have been attenuated in the same ratio as the O(1s) feature (e.g., $O(1s)_{post\text{-}exposure}$ /$O(1s)_{pre\text{-}exposure}$), and this was used in a fit to the post-exposure feature. In selected cases we also obtained spectra of the Ta(4d) region, and these results compared well to those found for the Ta(4f) peak, stripped of the O(2s) contribution.

In one set of experiments these scans were followed by the angle resolved scans for C(1s) and Si(2p) for depth profiling of the IOL while in the other set of experiments, initial scans were followed by the $Ta[N(CH_3)_2]_5$ exposure. This method ensured that the damage to the IOLs due to prolonged exposure to X-rays was not manifested in the $Ta[N(CH_3)_2]_5$ exposure experiments reported in the present work. [16] The surfaces were exposed to $Ta[N(CH_3)_2]_5$ for a period of 3 hours which was found to be sufficient to saturate the surface completely. After exposure, the Ta(4f) spectrum was obtained to quantify the amount of Ta adsorbed on the surface. This spectrum was subsequently fit to two peaks, corresponding to O(2s) and Ta(4f) features as described above. A post exposure N(1s) spectrum was obtained for calculations of the stoichiometry of the adlayer while C(1s), O(1s) and Si(2p) spectra were obtained to determine

the impact of $Ta[N(CH_3)_2]_5$ exposure on the IOL. Angle resolved spectra for the Ta(4f) feature was also obtained to determine the spatial extent of the reaction.

In order to quantify the XPS data, a polycrystalline Au reference standard was used to obtain a Au(4f) peak. This reference sample was made by depositing 2000 Å of a Au film on a Si(100) wafer with a native oxide on the surface, using 100 Å of a Cr film in between as the adhesion layer. The Cr and Au films were deposited using e-beam evaporation.

S.III Results and discussion

S.III.A Characterization of the organic layers

i. Model for Gen-0 and Gen-1 layers

The spectra for the C(1s) feature may be used to estimate the absolute density of the Gen-0 IOLs, and the absolute density that is added in the Gen-1 step. In the former case, assuming that hydroboration of the nitrile group is complete (for 12C), there is a one-to-one correspondence between the Gen-0 IOL density and that of terminal $–NH_2$ groups. In the latter case, if certain assumptions are made as to the nature and success of the branching step, then we can also make an estimate of the terminal $–NH_2$ groups for the Gen-1 IOLs. In order to make absolute estimates in XPS, one needs an absolute reference standard. We use a polycrystalline Au sample and the Au($4f_{7/2}$) peak. In addition, one needs to account for the following factors that affect the intensity: the photoelectron cross-sections, σ, for sample [C(1s)] and reference [Au($4f_{7/2}$)] peaks; the analyzer transmission function, T(E) (inversely proportional to the kinetic energy); the atomic density of the two elements, N, and the inelastic mean free path, λ, for the photoelectrons. Concerning these, $\sigma_{Au}/\sigma_C = 9.8$ [5], $N_{Au} = 5.88 \times 10^{22}$ atoms-cm^{-3} [17] and $\lambda_{Au} = 15.5$

Å [18]. The atomic density of C in the IOL/SAM depends on its areal density, n_{SAM} (molecules-cm^{-2}), and the mean spacing between C in the backbone, d_C. The integrated intensity of the Au ($4f_{7/2}$) peak from the thick Au thin film is proportional to $\sigma_{Au} N_{Au} \lambda_{Au} T(E_{Au})$. For the C(1s) peak from the organic layers we must account for their finite thickness. In the case of the Gen-0 IOLs for 3C and 12C, we assume they form uniform layers of constant thickness and constant density of C. The integrated intensity of the C(1s) peak from such a layer is proportional to:

$$I_0 [1 - \exp (-n\, d_C / \lambda_C \cos \theta)], \qquad \text{[S-1]}$$

where $I_0 = \sigma_C (n_{SAM}/d_C) \lambda_C T(E_C)$, n is the number of carbons in the IOL/SAM backbone (equivalently $n\, d_C$ is the thickness of the IOL) and θ is the takeoff angle.

For the Gen-1 IOLs we use a bilayer model, where again both layers are uniform, constant thickness and constant density of C. In this case the integrated intensity is proportional to the sum of two terms:

$$\sigma_C (n_{SAM2}/d_{C2}) \lambda_{C2} T(E_C) [1 - \exp (-n\, d_{C2} / \lambda_{C2} \cos \theta)]; \qquad \text{[S-2(a)]}$$

and

$$\exp[-n\, d_{C2} / \lambda_{C2} \cos \theta]\, \sigma_C (n_{SAM1}/d_{C1}) \lambda_{C1} T(E_C) [1 - \exp (-n\, d_{C1} / \lambda_{C1} \cos \theta)] \qquad \text{[S-2(b)]}$$

The term in Eq. [S-2(a)] represents the integrated intensity contributed from the organic layer made in the Gen-1 step (identical in form to Eq. [S-1]), while the term in Eq. [S-2(b)] represents the contribution from the Gen-0 step with the additional exponential term accounting for the

attenuation of the photoelectrons due to the Gen-1 layer (SAM2) that lies on top of the Gen-0 layer (SAM1).

ii. ARXPS of C(1s)

Key in these calculations is having knowledge of, or making an estimate for, the inelastic mean free path of the C(1s) photoelectrons. These can be obtained via the use of the angle resolved XPS (ARXPS). In Fig. S-1 we plot the integrated peak areas for the C(1s) feature as a function of take-off angle for the layers anchored by (a) 3C and (b) 12C. Here, for Gen-0, we fit the data to the model that assumes a single organic layer is present, uniform in thickness, and with a constant density of C, i.e., Eq. [S-1]. This fit gives $n\ d_C/\ \lambda_C$. Using the ellipsometric thicknesses for Gen-0 3C and Gen-0 12C reported in Table 1 in the main text (for $n\ d_C$), from the fit we find $\lambda_{Gen\text{-}0} = 40.4 \pm 26.1$ Å for 3C and 23.8 ± 13.9 Å for 12C. For the Gen-1 organic layer we fit the data to a bilayer model described above, the sum of Eqs. [S-2(a)] and [S-2(b)]. Here to restrict the number of parameters, we use the results from the fit to the Gen-0 layer for two sets of terms in Eq. [S-2(b)] [I_0 is used for $\sigma_C\ (n_{SAM1}/d_{C1})\ \lambda_{C1}\ T(E_C)$, and $n\ d_C/\ \lambda_C$ is used for $n\ d_{C1}/\ \lambda_{C1}$], in the fit to the data for Gen-1 layer. In addition, for the thickness added by the Gen-1 layer [$n\ d_{C2}$], we use that found from ellipsometry also given in Table 1 in the main text. With these restrictions from the fit we find $\lambda_{Gen\text{-}1} = 16.4 \pm 13.3$ Å for 3C and 13.6 ± 13.2 Å for 12C.

iii. density calculation

Making use of these values for the inelastic mean free paths, we can calculate the density of the organic layers formed in the Gen-0 and Gen-1 steps. These values are given in Table 1 in

the main text. Given the assumptions we have made here and the experimental uncertainties, we estimate the absolute accuracy of these values to be ± 30%.

iv. ARXPS of Si(2p)

A final set of analyses we have conducted on the substrates possessing the organic layers only is XPS of the Si(2p) region. As chemically oxidized Si is the starting substrate for all cases, formation of overlayers should result in the attenuation of these photoelectrons from the Si(2p). We consider results for both (large aperture) single take-off angle XPS, and (small aperture) angle-resolved XPS. In Fig. S-2 we plot the Si(2p) spectra for three surfaces: the chemically oxidized Si, and the same surface modified with Gen-0-3C and Gen-1-12C organic overlayers. As may be seen, both organic overlayers attenuate the Si substrate peak, and the attenuation is stronger for the thicker Gen-1-12C layer. Also displayed in the inset of Fig. S-2, is the ratio of the integrated intensity for the Si(2p) peak for the surfaces with organic overlayers with respect to that of the starting chemical oxide, plotted as a function of the ellipsometric thickness. As may be seen there is increased attenuation as a function of ellipsometric thickness. From the slope of these data one can estimate the inelastic mean free path of the Si(2p) photoelectrons through the four layers, via . $\lambda_{Si} = [(-\Delta \ln I/\Delta d) \cos \theta]^{-1}$. From these data we find values of 46 Å (Gen-0-3C), 36 Å (added Gen-1-3C layer), 68 Å (Gen-0-12C), and 22 Å (added Gen-1-12C layer) (solid line shows combined fit, giving 37 Å). The absolute values are of less concern here than the change, as a decrease in λ_{Si} would indicate formation of a denser layer. Indeed, in both cases there is a decrease in λ_{Si} in going from Gen-0 to Gen-1, and the decrease is larger in the case of 12C. This is again evidence for a more efficient Gen-1 conversion from the 12C anchor.

We have also examined the Si(2p) feature using ARXPS. In Fig. S-3 we plot the integrated peak areas for the Si(2p) feature as a function of take-off angle for the layers anchored by (a) 3C and (b) 12C. Qualitatively, it may be seen that there is a reduction in the integrated peak intensities at all take-off angles when comparing the results from Gen-0 to Gen-1. This is of course consistent with the expectation for higher attenuation of the Si(2p) photoelectrons due to a thicker (and denser) molecular layer formed in the Gen-1 step. These data can be modeled as phototemission from a semi-infinite substrate that is covered by a uniformly thick thin (organic) film: $I_0 \exp(-d / \lambda \cos\theta)$, where, I_0 is the unattenuated emission from the substrate. This analysis was used to interpret the data shown in the inset in Fig. S-2. In fitting these data I_0 was assumed to be constant for all four cases. For the parameter d/λ we find values of 0.35 (Gen-0-3C), 0.53 (Gen-1-3C), 0.33 (Gen-0-12C), and 0.45 (Gen-1-12C). For both anchors we see that there is increased attenuation (larger d/λ) when going from Gen-0 to Gen-1. This is additional evidence for the effectiveness of the Gen-1 step.

v. AFM of IOLs

Atomic force microscopy has been used to investigate the surface morphology before and after growing the Gen-0 and Gen-1 organic layers. In Fig. S-4 we display AF micrographs for bare SiO_2 (chemical oxide), Gen-0-12C and Gen-1-3C. The starting chemical oxide was found to be smooth and featureless with a root mean square (RMS) surface roughness of 4.21 Å. After deposition of Gen-0-12C the surface roughness increased only marginally to 4.44 Å, which could be considered essentially equivalent to the starting surface given experimental uncertainties. After growth of Gen-1-3C the surface roughness was also found to be in this range; namely 4.29

Å. Of note, in both cases there seems to be little if any evidence for pinhole or other types of defects in the organic layers.

S.III.B. Reaction of the organic layers with Ta and Ti coordination complexes

i. adsorption kinetics and saturation exposure

Having characterized the organic layers we now move on to an examination of their reactivity with two transition metal coordination complexes. We expect these complexes to react with the terminal $–NH_2$ groups (and possibly the -NH- groups, *vide infra*) via ligand exchange reactions.[15] We consider first the reaction with $Ta[N(CH_3)_2]_5$. In this work the surfaces with the organic layers were exposed to the Ta complex at room temperature in the ultrahigh vacuum chamber. In-situ XPS has been used to characterize the reactions between the Ta complex and the organic layers. In Fig. S-5 we display the coverage exposure relationship for $Ta[N(CH_3)_2]_5$ on a Gen-0-12C layer. Here the Ta(4d) feature was used to measure the coverage of chemisorbed Ta. The smooth curve represents a fit to first-order Langmuirian kinetics—we see that this describes the data well. From these data, and knowledge of the absolute coverage (vide infra) and the flux of incident molecules we calculate an initial probability of reaction of 0.028 ± 0.005 based on the quality of the fit. (The actual experimental uncertainty in the absolute value is larger, i.e., about 50%.) This value is similar (within an order of magnitude) to those we have measured for thermal energy and molecular beam (E_i = 0.63 eV) exposures of $Ti[N(CH_3)_2]_4$ to this same Gen-0-12C, $–NH_2$ terminated SAMs, where we found absolute values of 0.13 ± 0.04 [15], and 0.33 ± 0.04 [19]. It is also similar to that measured for $Ti[N(CH_3)_2]_4$ on a $-N(i\text{-}C_3H_7)H$ terminated SAMs, where we found values of 0.024-0.028. [20] We have also measured the coverage exposure relationship for $Ta[N(CH_3)_2]_5$ on a Gen-1-12C layer. In this case also we find

that the data are well described by first-order Langmuirian kinetics and that the initial probability of reaction is about 0.028 ± 0.007, essentially the same as that for Gen-0-12C.

In Fig. S-6, we display the XP spectra for the Ta(4d) features after a saturation adsorption of PDMAT on the organic layers. As may be seen from this figure (as well as Fig. 4 in main text), on both surfaces there is a significant increase in intensity going from Gen-0 to Gen-1. On the 3C layer the ratio of integrated intensities, $I_{\text{Ta(4f), Gen-1-3C}}/I_{\text{Ta(4f), Gen-0-3C}}$, is 2.03, while that on the 12C layer, $I_{\text{Ta(4f), Gen-1-12C}}/I_{\text{Ta(4f), Gen-0-12C}}$, is 2.41. Analysis of the Ta(4d) spectra give similar increases in the amount of chemisorbed Ta in going from Gen-0 to Gen-1, namely a factor of 1.92 on the 3C anchor, and 2.26 on the 12C anchor. This of course correlates with our estimates that the Gen-1 layers have a higher density of terminal $-NH_2$ groups. These results strongly support that the saturation coverage of the Ta complex is a strong function of the density of the terminal $-NH_2$ groups. As explained in the main text, Ta(4d) spectra have also been used to study peak shifts to obtain details about possible reaction stoichiometries.

ii. adlayer microstrcuture

As a final point of discussion concerning the reactivity of the organic layers with the Ta and Ti complexes we will consider the stoichiometry of the adlayers that are formed. First as discussed above, due to the greater intensity of the C(1s) feature we have used it to estimate the density of terminal functional groups. For both Gen-0 layers this is unlikely to be problematic, while for the Gen-1 layers certain nonidealities can introduce errors in this calculation. Let us assume for the moment that this procedure gives us the correct density for terminal functional groups. In Fig. S-7 we plot the saturation density of the transition metal coordination complexes vs. the (expected) density of terminal functional groups. Here, for the former, we do not

compensate for attenuation of the photoelectrons emanating from the transition metal. As may be seen in the figure, there is a strong correlation between the density of the terminal functional groups and the saturation density of the metals. In terms of the number of functional groups that appear to have reacted with the transition metal coordination complexes via ligand exchange reactions, the number ranges from 1.63 ± 0.34 to 2.74 ± 0.86 for the Ta complex, whereas it is approximately 1.59 ± 0.51 for the Ti complex. For the sake of argument, if we take this number as 2 for both cases, it is very comparable to results we have found previously for reaction of $Ti[N(CH_3)_2]_4$ with Gen-0-12C [15] and for the reaction of this same molecule with oligo(phenylene-ethynylene) SAMs possessing an isopropyl termination [20]. Also, it suggests two possible scenarios: only ½ of the total terminal $–NH_2$ groups have reacted with the transition metal complexes, or each complex has reacted with 2 $–NH_2$ groups.

References

1. LiebmannVinson, A.; Lander, L. M.; Foster, M. D.; Brittain, W. J.; Vogler, E. A.; Majkrzak, C. F.; Satija, S. *Langmuir* **1996**, 12, 2256-2262.
2. Sung, M. M.; Kluth, G. J.; Maboudian, R. *J. Vac. Sci. Technol., A* **1999**, 17, 540-544.
3. Wasserman, S. R.; Tao, Y. T.; Whitesides, G. M. *Langmuir* **1989**, 5, 1074-1087.
4. Moon, J. H.; Shin, J. W.; Kim, S. Y.; Park, J. W. *Langmuir* **1996**, 12, 4621-4624.
5. Brzoska, J. B.; Benazouz, I.; Rondelez, F. *Langmuir* **1994**, 10, 4367-4373.
6. Balachander, N.; Sukenik, C. N. *Langmuir* **1990**, 6, 1621-1627.
7. Tomalia, D. A.; Baker, H.; Dewald, J.; Hall, M.; Kallos, G.; Martin, S.; Roeck, J.; Ryder, J.; Smith, P. *Polym. J.* **1985**, 17, 117-132.
8. Tomalia, D. A.; Baker, H.; Dewald, J.; Hall, M.; Kallos, G.; Martin, S.; Roeck, J.; Ryder, J.; Smith, P. *Macromolecules* **1986**, 19, 2466-2468.
9. Padias, A. B.; Hall, H. K.; Tomalia, D. A.; Mcconnell, J. R. *J. Org. Chem.* **1987**, 52, 5305-5312.
10. *Handbook of Optical Constants of Solids,* Palik, E. D., Ed.; Academic Press: New York, 1985.
11. Shirley, D. A. *Phys. Rev. B* **1972**, 5, 4709-&.
12. *Practical Surface Analysis: Volume I, Auger and X-Ray Photoelectron Spectroscopy,* 2 ed.; Seah, M. P.; Briggs, D., Eds.; John Wiley and Sons: Chichester, England, 1990.
13. Conny, J. M.; Powell, C. J. *Surf. Interface Anal.* **2000**, 29, 856-872.
14. Xia, L. Q.; Jones, M. E.; Maity, N.; Engstrom, J. R. *J. Vac. Sci. Technol., A* **1995**, 13, 2651-2664.

15. Killampalli, A. S.; Ma, P. F.; Engstrom, J. R. *J. Am. Chem. Soc.* **2005**, 127, 6300-6310.

16. Frydman, E.; Cohen, H.; Maoz, R.; Sagiv, J. *Langmuir* **1997**, 13, 5089-5106.

17. *Solid State Physics,* Ashcroft, N. W.; Mermin, N. D.; Harcourt Brace College Publishers: U.S.A., 1976.

18. Powell, C. J.; Jablonski, A. *J. Vac. Sci. Technol., A* **1999**, 17, 1122-1126.

19. Ma, P.F.; Dube, A.; Killampalli, A,; Engstrom, J.R. *J. Chem. Phys.* **2006**, 125, 034706-1/12.

20. Dube, A.; Chadeayne, A. R.; Sharma, M.; Wolczanski, P. T.; Engstrom, J. R. *J. Am. Chem. Soc.* **2005**, 127, 14299-14309.

Figure Captions

Figure S-1 Peak area of the C(1s) region for both the Gen-0 (○) and Gen-1 (■) layers of (a) 3C, and (b) 12C as a function of take-off angle. The smooth curves are fits to models described in the text, namely Eqs. [S-1], [S-2(a)], [S-2(b)].

Figure S-2 XP spectra of the Si(2p) feature for: bare chemical oxide (the starting substrate); the thinnest (Gen-0-3C) and the thickest (Gen-1-12C) organic layer examined here. The inset shows attenuation of the area of the Si(2p) peak by the organic layers as a function of their thickness, measured by ellipsometry. The solid line is a fit of the combined data set to model assuming exponential attenuation.

Figure S-3 Peak area of the Si(2p) region for both the Gen-0 (○) and Gen-1 (■) layers of (a) 3C, and (b) 12C as a function of take-off angle. The smooth curves are a fit to a model that assumes the SiO_2 substrate is covered by an organic film of uniform thickness.

Figure S-4 Atomic force micrographs of three surfaces: (a) bare chemical oxide: 500 nm × 500 nm; (b) Gen-0-12C: 300 nm × 300 nm; and (c) Gen-1-3C: 500 nm × 500 nm. The RMS roughness is ~ 4Å for all surfaces.

Figure S-5 Coverage-exposure relationship deduced from XPS for the adsorption of $Ta[N(CH_3)_2]_5$ on Gen-0-12C at T_s = 25 °C. The ordinate represents the integrated

area under the Ta(4d) feature. The flux of the incident $Ta[N(CH_3)_2]_5$ was 1.2×10^{12} molecules-cm^{-2}-s^{-1}. The smooth curve is the fit of the data to first-order Langmuirian kinetics.

Figure S-6 XP spectra of the Ta(4d) feature following saturation exposures of both the Gen-0 (○) and Gen-1 (■) layers of (a) 3C, and (b) 12C to $Ta[N(CH_3)_2]_5$ at T_s = 25 °C. The spectra have been fit to two peaks ($4d_{5/2}$, $4d_{3/2}$), corresponding to the split produced by the spin-orbit coupling.

Figure S-7 The atomic ratio, N:M, vs. the ratio of the OFG (terminal organic functional group, $-NH_2$):M for saturated adlayers. Open symbols represent results on the Gen-0 layers; filled on the Gen-1 layers. For the ordinate, the density of metal used is that given Table III in the main text (attenuation uncorrected).

Figure S-1

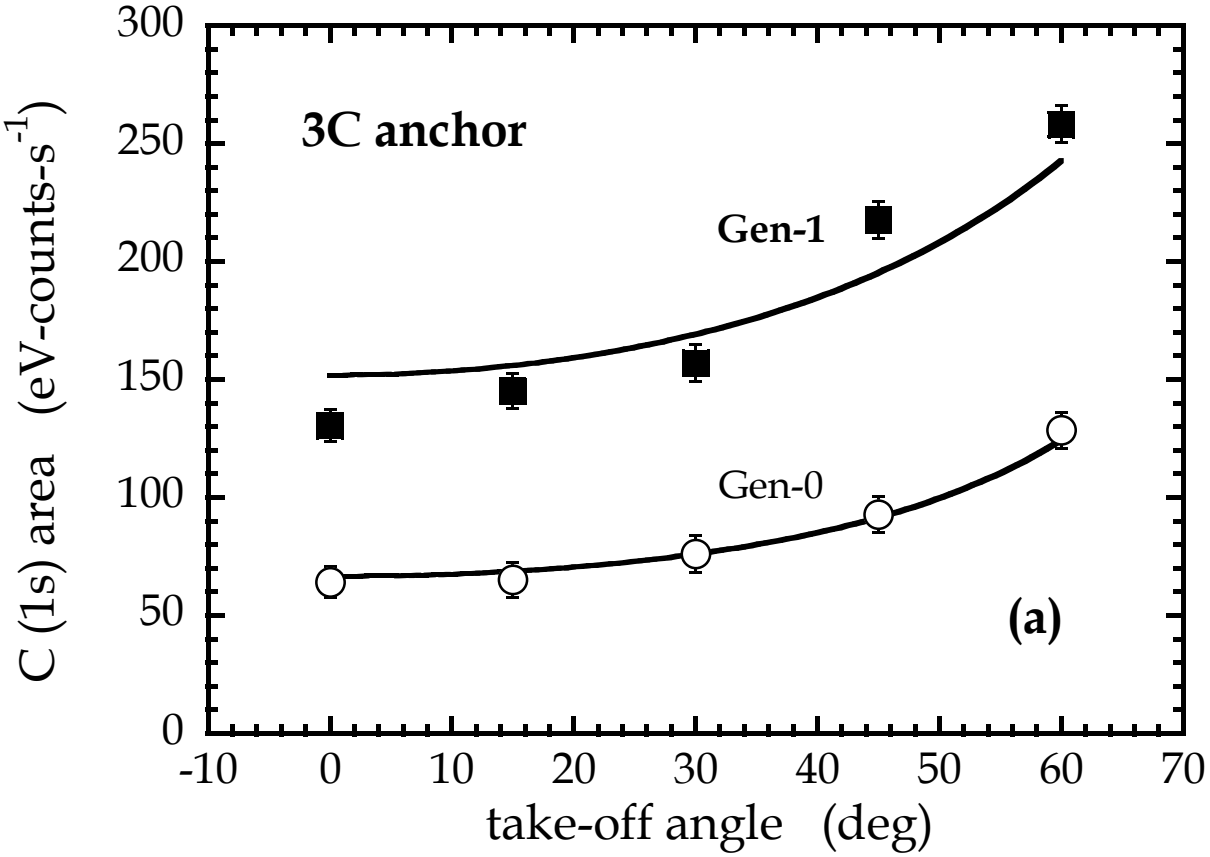
3C anchor
Gen-1
Gen-0
(a)
C (1s) area (eV-counts-s^{-1})
take-off angle (deg)
300
250
200
150
100
50
0
-10
0
10
20
30
40
50
60
70

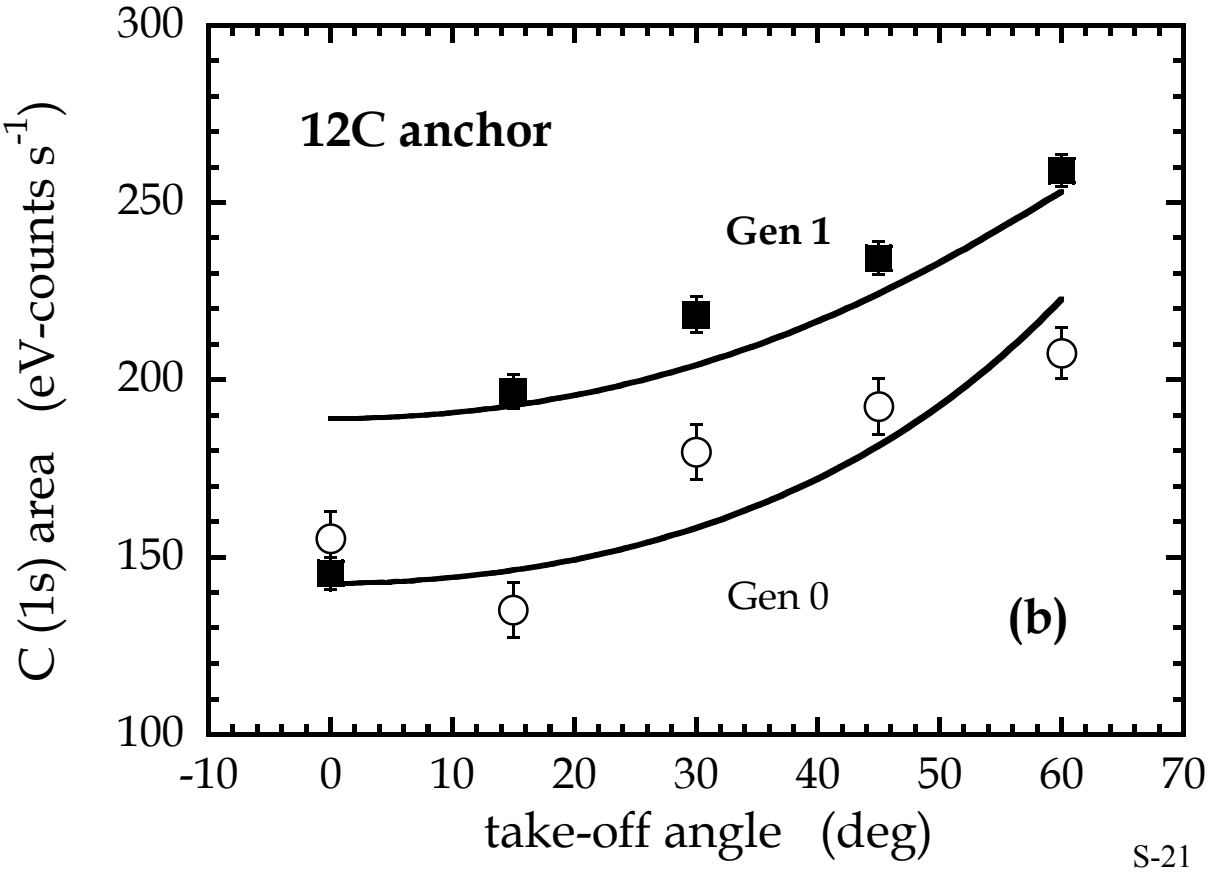
12C anchor
Gen 1
Gen 0
(b)
C (1s) area (eV-counts s^{-1})
take-off angle (deg)
300
250
200
150
100
-10
0
10
20
30
40
50
60
70

Figure S-2

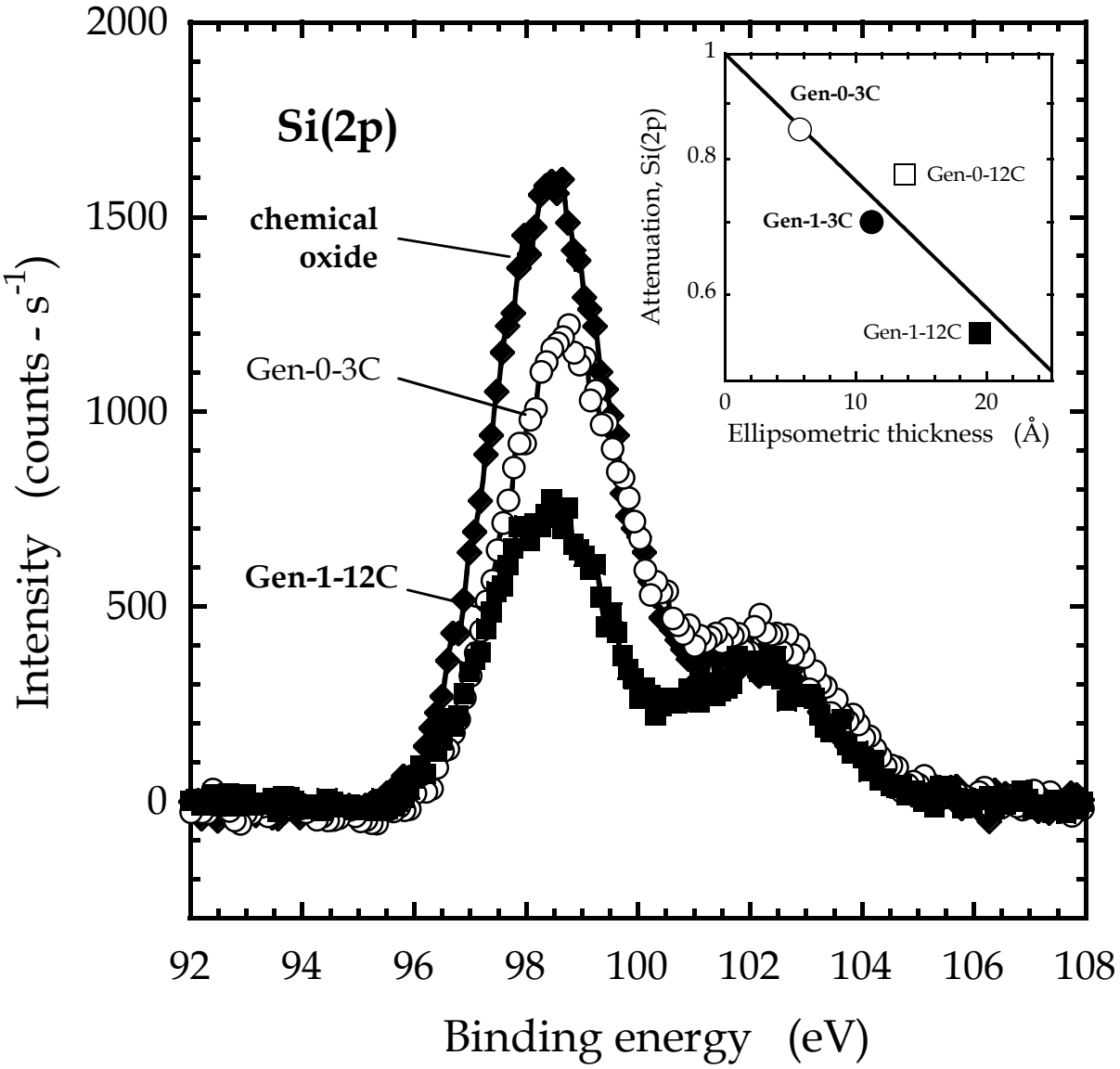
Si(2p)
chemical oxide
Gen-0-3C
Gen-1-12C
Intensity (counts - s-1)
Binding energy (eV)
2000
1500
1000
500
0
92
94
96
98
100
102
104
106
108
Attenuation, Si(2p)
1
0.8
0.6
Gen-0-3C
Gen-0-12C
Gen-1-3C
Gen-1-12C
0
10
20
Ellipsometric thickness (Å)

Figure S-3

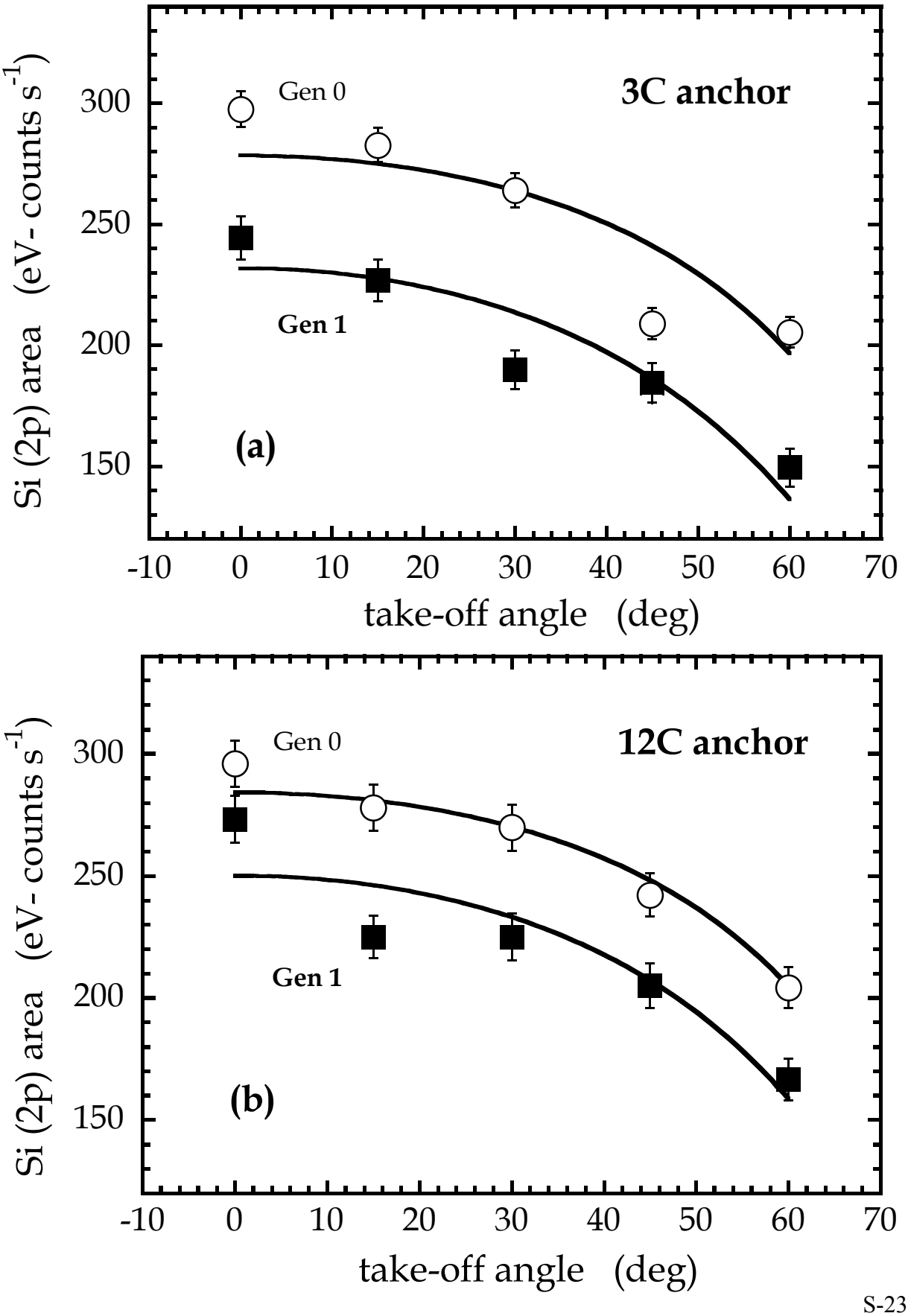
Gen 0
3C anchor
Gen 1
(a)
Si (2p) area (eV- counts s-1)
300
250
200
150
-10
0
10
20
30
40
50
60
70
take-off angle (deg)
Gen 0
12C anchor
Gen 1
(b)
Si (2p) area (eV- counts s-1)
300
250
200
150
-10
0
10
20
30
40
50
60
70
take-off angle (deg)

Figure S-4

(a)

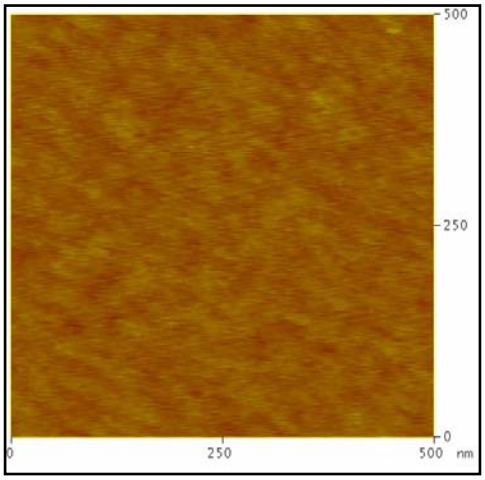

(b)

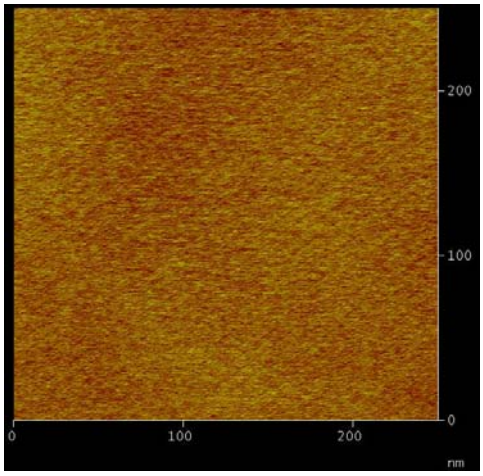

(c)

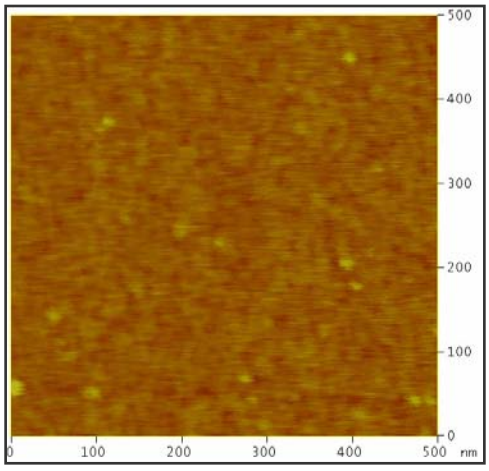

Figure S-5

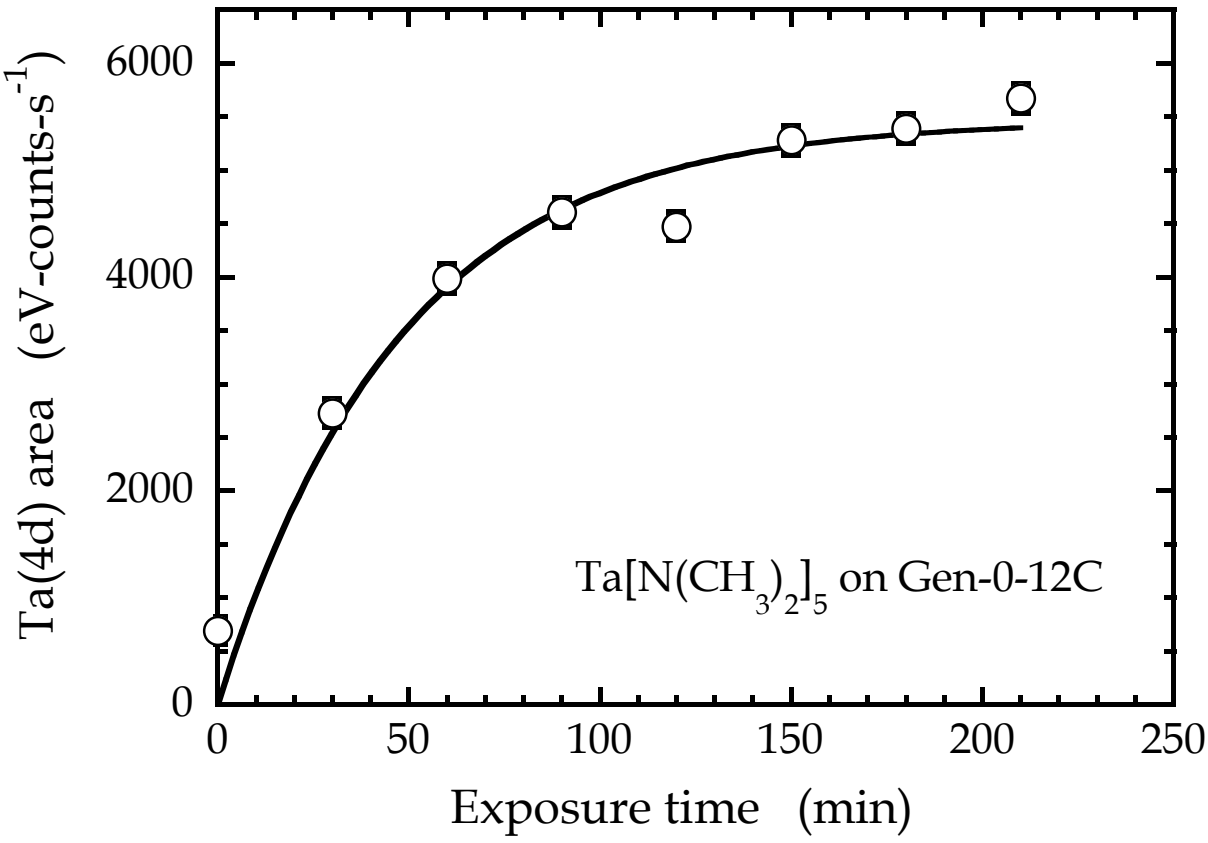
Ta(4d) area (eV-counts-s-1)
6000
4000
2000
0
0
50
100
150
200
250
Exposure time (min)
Ta[N(CH3)2]5 on Gen-0-12C

Figure S-6

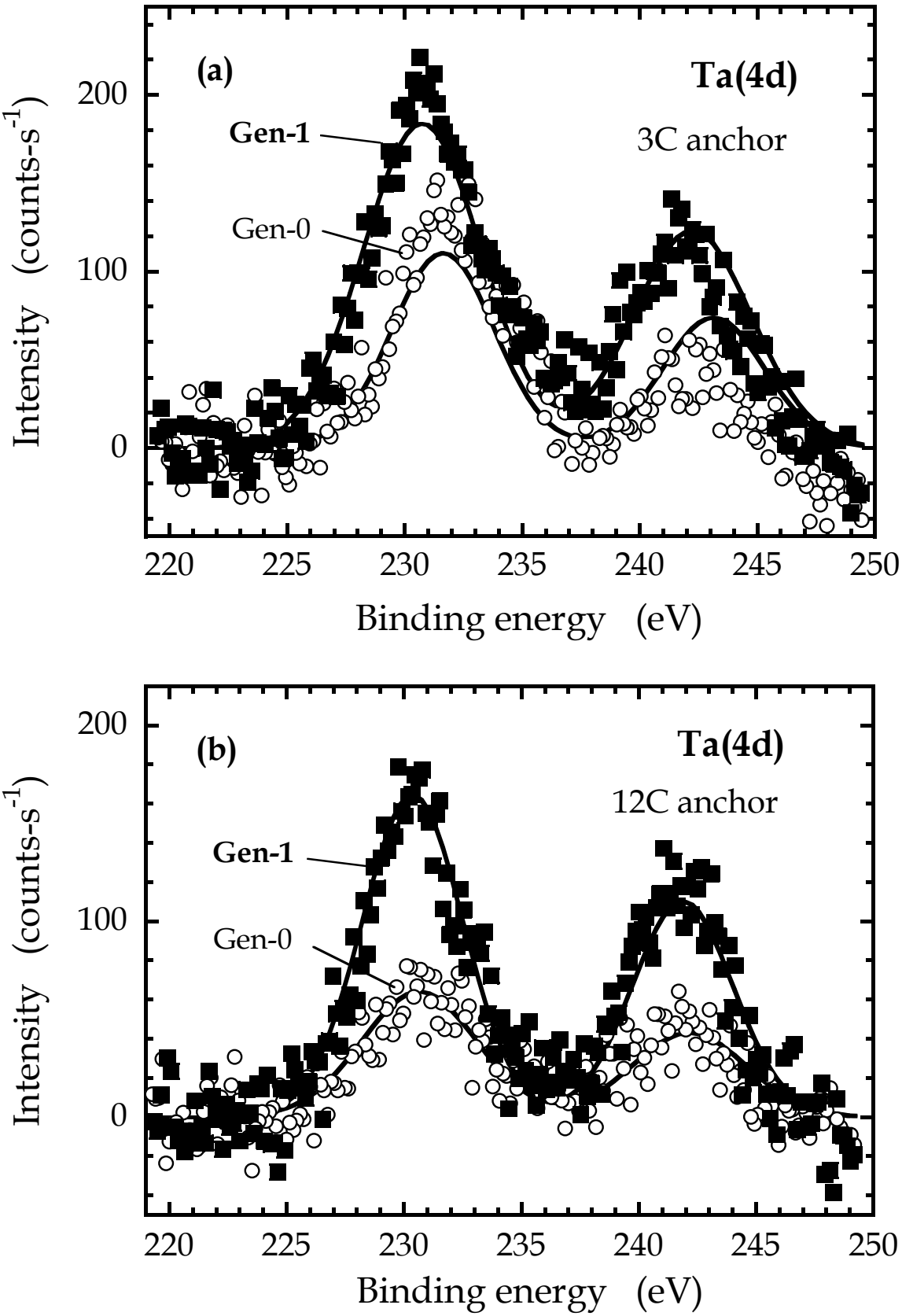
(a)
Ta(4d)
3C anchor
Gen-1
Gen-0
Intensity (counts-s-1)
200
100
0
220
225
230
235
240
245
250
Binding energy (eV)
(b)
Ta(4d)
12C anchor
Gen-1
Gen-0
Intensity (counts-s-1)
200
100
0
220
225
230
235
240
245
250
Binding energy (eV)

Figure S-7

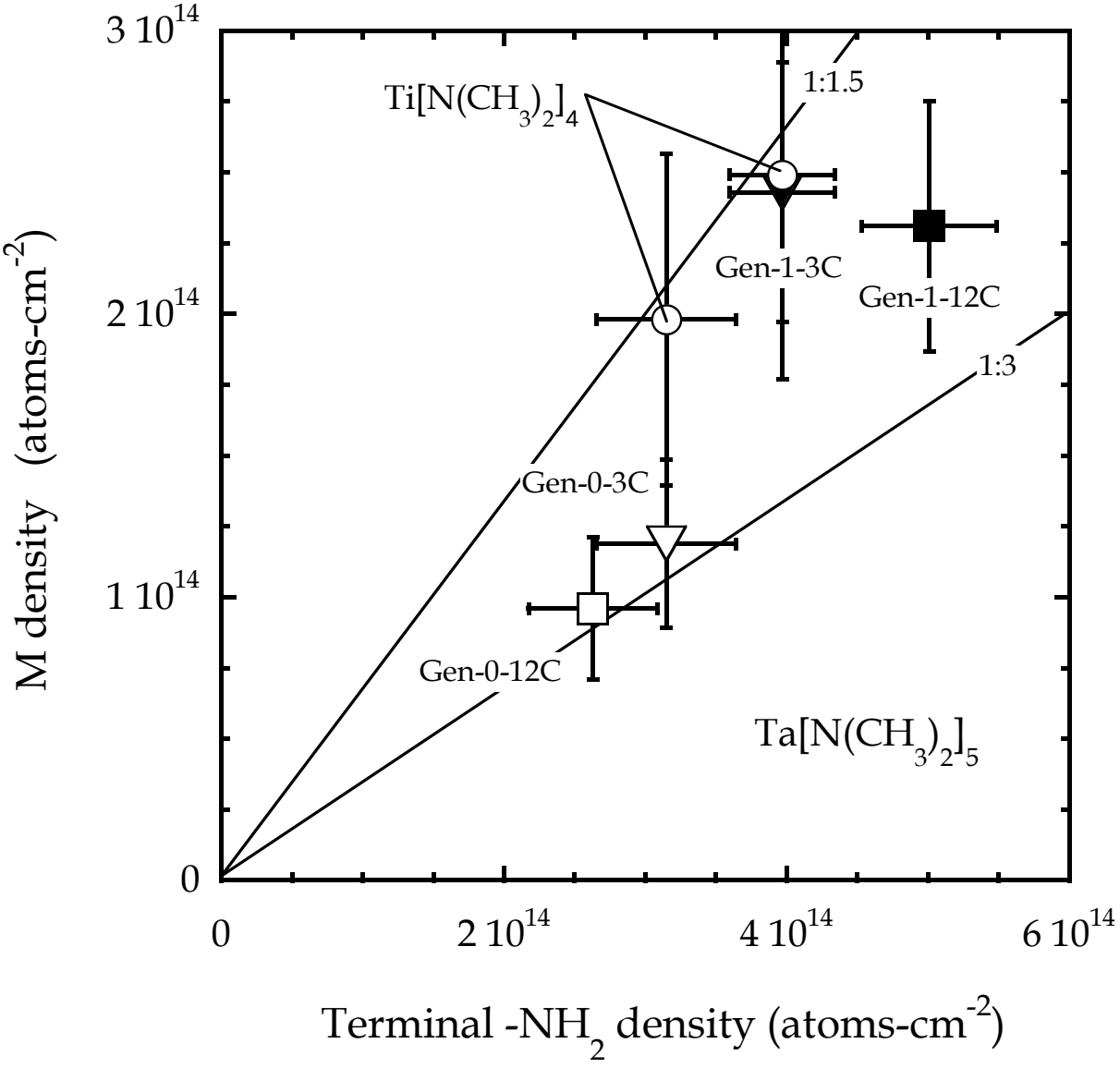
3 10^14
2 10^14
1 10^14
0
M density (atoms-cm^-2)
Ti[N(CH3)2]4
1:1.5
Gen-1-3C
Gen-1-12C
1:3
Gen-0-3C
Gen-0-12C
Ta[N(CH3)2]5
0
2 10^14
4 10^14
6 10^14
Terminal -NH2 density (atoms-cm^-2)